

# DESIGN OF A PITCH-ROLL JOYSTICK BASED ON THREE LOBE SPHERICAL CAM MECHANISM

Debal Saha, Jorge Angeles, Jozsef Kövecses  
*Department of Mechanical Engineering, McGill University, Montréal, Canada.*  
*Email: debalsaha@cim.mcgill.ca; jorge.angeles@mcgill.ca; jozsef.kovecses@mcgill.ca*

---

## ABSTRACT

A pitch-roll joystick based on spherical cam mechanism is proposed that can be implemented as a haptics device. Spherical cams can replace bevel gears that are conventionally used in transmission mechanisms involving shafts with intersecting axes to achieve lower backlash, lower frictional losses and higher stiffness. Such a spherical cam mechanism essentially comprises of multi-lobe-cams and conical rollers that allows two degrees-of-freedom. Undercutting is a deterrent to the generation of smooth cam surface and necessitates synthesis of a singularity free spherical cam profile. The issues of high pressure angle and maintaining a high contact ratio is addressed by having a cam with more than one lobe. The design of the cam profile and the assembly of the joystick is described. The criteria for the selection of number of lobes and rollers is also explained. The results of the kinematic simulation of the joystick are also presented.

**Keywords:** spherical multi-lobe cam ; pitch-roll joystick ; pressure angle.

---

## LA CONCEPTION D'UN MANCHE À BALAI TANGAGE-ROULIS BASÉE SUR UN MÉCANISME À CAMES SPHÉRIQUES À TROIS LOBES

### RÉSUMÉ

Les mécanismes à cames sphériques peuvent remplacer les engrenages coniques car ils offrent un jeu et des pertes dues au frottement plus faibles que ces derniers, tout en augmentant la rigidité de l'ensemble. Ces mécanismes sont essentiellement composés de cames multilobes et de roulements coniques qui permettent deux degrés de liberté. Pour éviter la contre-dépouilles, il faut synthétiser un profil de came sphérique libre de singularités. Les cames à plusieurs lobes permettent de résoudre le problème posé par un angle de pression et un rapport de contact trop élevés. Les auteurs proposent un manche à balai tangage-roulis basé sur un mécanisme à cames de type sphérique qui puisse servir de dispositif haptique. Ils traitent de la conception du profil de la came, de l'assemblage du manche à balai et du choix du nombre de lobes et de lobes et de roulements. Ils présentent les résultats de la simulation cinématique du manche à balai.

**Mots-clés :** came sphérique multilobes ; manche à balai tangage roulis ; angle de pression.

## 1. INTRODUCTION

The traditional method employed for transmission between two perpendicular shafts is one via bevel gears. There are some inherent drawbacks like high backlash and high friction that renders the use of bevel gears for transmission specific to applications like that in robotic wrists and haptics devices, incapable of delivering desired level of performance. Spherical cam mechanisms provide suitable substitutes for bevel gears, as observed by Bai and Angeles [1]. A cam-follower mechanism is proposed here that is essentially composed of a spherical cam and a follower with conical rollers. The rollers and the cam constitute a higher kinematic pair which provide favorable features to the cam mechanism, like high stiffness, high contact ratio, low friction and low backlash. Various other advantages that spatial cam mechanisms, in general, possess over conventional drive-transmission mechanisms are cited by Wei et al. [6].

A pitch-roll joystick based on a spherical cam mechanism is proposed that is intended for haptic applications. The design of the various parts of the joystick are conceptualized based on the recommendations found in the literature [7–10], while developing joysticks for various purposes. The number of lobes and rollers for the multi-lobe cam (MLC) are decided to be three and four, respectively, as opposed to four and seven for a previous mechanism in [1], as this resulted in an optimal configuration with respect to joystick-design simplifications, resolving complexities in manufacturing and obtaining suitable values for cam-design parameters such as radius of curvature and pressure angle. Plots of cam profiles with three lobes and number of rollers varying from one to five are shown in Fig. 1.

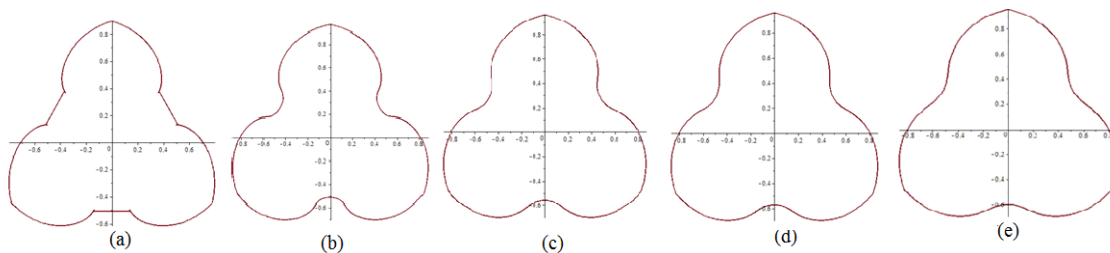


Fig. 1. cam-profiles for three lobes (a) one roller, (b) two rollers, (c) three rollers, (d) four rollers, (e) five rollers.

There are certain issues that need to be addressed while implementing spherical cam mechanism as a substitute for bevel gears. The singularities in cam profile leading to undercutting and a variable pressure angle are considered and resolved for better transmission in the proposed mechanism for the pitch-roll joystick. The transmission quality is also affected by the contact ratio; it is duly studied for the MLC case.

The assembly of the pitch-roll joystick implementing the cam-follower mechanism is then described, the mechanism performance assessed by kinematic simulation. Conclusions are then drawn for the suitability of the proposed joystick as a haptic device and other prospective applications.

## 2. GENERATION OF THE CAM PROFILE

The geometric fundamentals that govern the design and operation of cam mechanisms are studied under the branch of kinematic synthesis; they can be categorized in a specific class called cam synthesis. The principles that govern the kinematics of cam mechanisms are explained by describing the procedure for the generation of ruled surfaces.

The spherical curves required for cam-profile synthesis are generated by application of the *Aronhold-Kennedy Theorem*, which states that when three bodies are in relative motion, the three instant screw axes (ISAs), associated with the three pairs of bodies under relative motion, have one common perpendicular. In the case of spherical motion each ISA becomes an *Instant Axis* (IA) of rotation, all IAs intersecting at one common point, the centre of the spherical motion in question. The ruled surfaces generated by the rotation

of the IAs play a key role in the synthesis of the desired cam-profile.

The proposed spherical cam mechanism is a four-link mechanism comprising a spherical cam, a follower, a roller and a frame. To generate its cam profile, the IAs of the rotation of the links w.r.t. each other are identified first.

The nomenclature for the vectors and the angles useful for cam-profile generation is adopted from an earlier publication. A major difference between the foregoing reference and this paper is that the former provides a generally applicable methodology; the latter proposes one specific application targeting haptics. The design of interest relies on ergonomics data drawn from the specialized literature [7–10]. All the elements of a spherical cam mechanism are shown in Fig. 2 with their representative arcs.

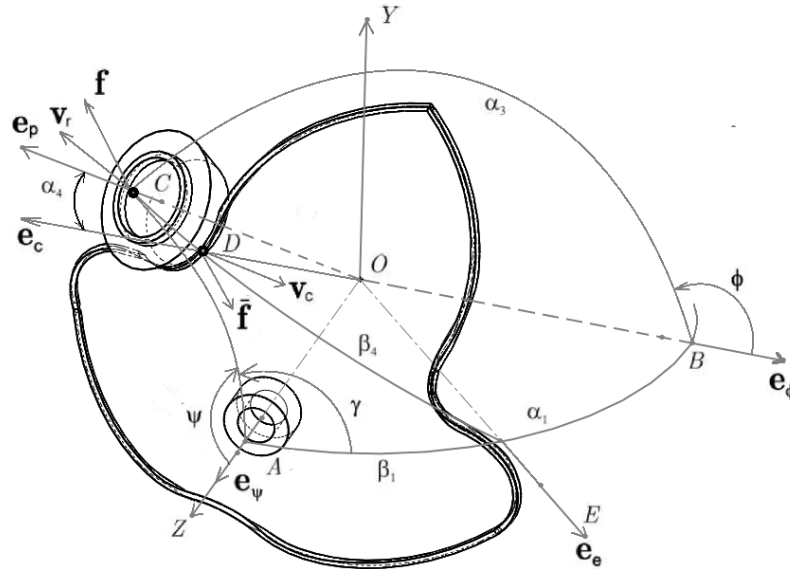


Fig. 2. Axes and angles defined for the spherical cam mechanism

Table 1. Definition of vectors used for cam-profile synthesis

Notation	Vector Definition
$e_\psi$	Vector parallel to the axis of the cam rotation w.r.t. the frame
$e_p$	Vector parallel to the roller-shaft axis
$e_c$	Vector parallel to the instant axis of rotation of the cam w.r.t the follower
$e_\phi$	Vector parallel to the follower shaft
$e_c$	Vector parallel to the axis of rotation of the roller w.r.t. the cam

The cam-profile is a conical surface with two spherical curves as its concentric boundaries, which are defined by the curves of intersection of the conical surface with two concentric spheres. The conical surfaces are generated by the spherical motion of the IA of rotation of the roller w.r.t. the cam. The position vector of an arbitrary point of these curves is given by an expression obtained by rotating a vector through the contact point of the roller with the cam about the cam axis (parallel to the Z-axis of the reference frame).

$M$  and  $N$  denote the number of lobes and rollers of roller-carrier, respectively, as needed in developing the kinematic relations relevant to cam profile generation and analysis for singularities and pressure-angle

Table 2. Angles used for cam-profile synthesis

Notation	Vector Definition
$\alpha_1$	Angle between the axis of the Cam and that of the roller carrier ( $\angle AOB$ )
$\alpha_3$	Angle subtended by arc of roller carrier ( $\angle BOC$ )
$\alpha_4$	Half angle subtended by conical roller ( $\angle COD$ )
$\beta_1$	Angle between the cam axis and the Instant Axis of rotation of the follower with respect to the cam ( $\angle AOE$ )
$\beta_4$	Angle between the axis of the roller and the instant axis of rotation of the follower w.r.t. cam ( $\angle COE$ )

distribution. The angles of rotation of the cam and the roller-carrier are represented by  $\psi$  and  $\phi$ , respectively. The input-output relation is given below:

$$\phi = -\frac{M}{N}\psi + \phi_0 \quad (1)$$

with  $M$  denoting the number of lobes and  $N$  the number of rollers.

The initial position of the cam (at  $\psi = 0$ ) is defined such that crest of one of its lobes lies on the axis (say at  $x = 0$ , or the  $Y$ -axis). We thus have  $\phi_0 = (1 - 1/N)\pi$ .

The first step for cam-profile generation is defining the reference frame required to represent the rotations of the various links. The global reference frame is defined as one fixed to the frame of the mechanism, with the  $Z$ -axis defined as the axis of rotation of the cam w.r.t. the frame. Using the nomenclature for the vectors along the axes of rotation and the angles subtended on the unit sphere shown in Fig. 2, the relations below follow:

1.  $\mathbf{e}_\psi = \mathbf{e}_z = [0 \ 0 \ 1]^T$
2.  $\mathbf{e}_p = \mathbf{Q}_y(\alpha_1) \mathbf{Q}_z(\phi) \mathbf{Q}_y(\alpha_3) \mathbf{e}_z$
3.  $\mathbf{e}_c = \mathbf{Q}_y(\beta_1) \mathbf{e}_z$
4.  $\mathbf{e}_\phi = \mathbf{Q}_y(\alpha_1) \mathbf{e}_z$

First, angle  $\beta_4$  is calculated,

$$\cos \beta_4 = \mathbf{e}_c^T \mathbf{e}_p \quad (2)$$

After expanding the right-hand side of Eq.(2), we obtain

$$\begin{aligned} \cos \beta_4 &= \sin \beta_1 \cos \alpha_1 \cos \phi \sin \alpha_3 + \sin \beta_1 \sin \alpha_1 \sin \alpha_3 \\ &\quad - \cos \beta_1 \sin \alpha_1 \cos \phi \sin \alpha_3 + \cos \beta_1 \cos \alpha_1 \cos \alpha_3 \end{aligned}$$

Further,  $\gamma$  is the angle of rotation of the conical roller about the instant axis of rotation  $OE$ , as shown in Fig. 2, and given by

$$\cos \gamma = \csc(\alpha_1 - \beta_1) \csc \beta_4 [\cos \alpha_3 - \cos(\alpha_1 - \beta_1) \cos \beta_4] \quad (3)$$

where  $\csc$  stands for cosecant.

The position vector  $s_c$  of a point on the spherical curve defining the profile is obtained by using vector  $\mathbf{e}_c$  and the rotation matrix  $\mathbf{Q}_z$  representing the rotation about the cam-axis through the angle of rotation of the cam,  $\psi$ , i.e.,

$$\mathbf{s}_c = \mathbf{Q}_z^T(\psi) \mathbf{e}_c = \begin{bmatrix} c\phi s\gamma s\beta_3 - s\psi(c\beta_1 c\gamma s\beta_3 + s\beta_1 c\beta_3) \\ s\psi s\gamma s\beta_3 - c\psi(c\beta_1 c\gamma s\beta_3 + s\beta_1 c\beta_3) \\ s\beta_1 c\gamma s\beta_3 + c\beta_1 c\beta_3 \end{bmatrix} \quad (4)$$

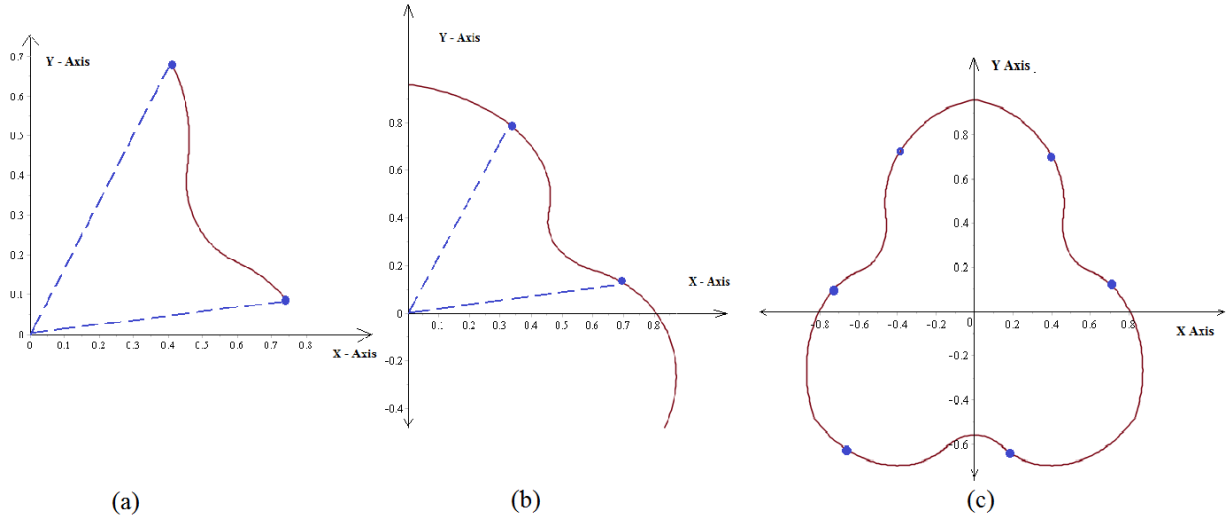


Fig. 3. (a) Complete pitch curve of the cam-profile when projected onto the  $X$ - $Y$  plane; (b) Complete cam-profile in two dimensions; (c) Conic surface defining the spherical cam-profile intersecting the sphere on which the spherical mechanism is based

where  $s$  stands for sine and  $c$  for cosine. With all the above relations simplified, the only variable of the position vector of the cam profile is the input angle  $\psi$  of the cam. In other words, we have the vector for the cam-profile generation as a function of  $\psi$ , given as  $\mathbf{s}_c = \mathbf{s}_c(\psi)$ . The projection of the cam-profile onto the  $X$ - $Y$  plane is shown in Fig. 3(c).

Similarly, the spherical curve generated using vector  $\mathbf{e}_p$  and the same rotation matrix for rotation about the cam-axis, called the *pitch curve*, is given by

$$\mathbf{s}_p = \mathbf{Q}_z^T(\psi)\mathbf{e}_p = \begin{bmatrix} s\psi s\phi s\alpha_3 + c\psi(c\alpha_1 c\phi s\alpha_3 + s\alpha_1 c\alpha_3) \\ c\psi c\phi s\alpha_3 - s\psi(c\alpha_1 c\phi s\alpha_3 + s\alpha_1 c\alpha_3) \\ s\alpha_1 c\phi s\alpha_3 + c\alpha_1 c\alpha_3 \end{bmatrix} \quad (5)$$

The position vector of the pitch curve obtained above is used to obtain an expression for the *radius of curvature* of the cam-profile.

The cams of the proposed spherical cam mechanism are designed with three lobes, i.e.,  $M = 3$ . The curve generated by Eq.(4) is incomplete; it needs to be defined for an extended range of  $\psi$ , which requires finding an *extension angle*  $\sigma$ , that is obtained by solving the equation  $\mathbf{s}_c(\psi)|_{\psi=\sigma} = \mathbf{0}$ . The plot of the extended curve is obtained for  $\psi \in [-2\pi/M - \sigma, \sigma]$ , as shown in Fig. 3(b).

The extended curve is then rotated  $M - 1$  times more, about the origin, through an angle of  $120^\circ$  to obtain the complete two dimensional cam-profile, as shown in Fig. 3(c). Computer algebra is used to manipulate the relations between the various variables and parameters of the mechanism, from which the position vector of an arbitrary point of the pitch curve of the cam-profile is obtained. The spherical curve representing the cam profile is shown in Fig. 4, obtained as the intersection of the conical surface of the cam with the sphere on which the spherical mechanism is based.

### 3. SINGULARITIES AND UNDERCUTTING AVOIDANCE

The study of singularities is vital, as singularities are the vulnerable points where *undercutting* may occur. *Undercutting* is the recess at a point in an otherwise smooth profile where there is an abrupt change of curvature due to presence of singularities like double points or cusps. To avoid *undercutting*, a limiting

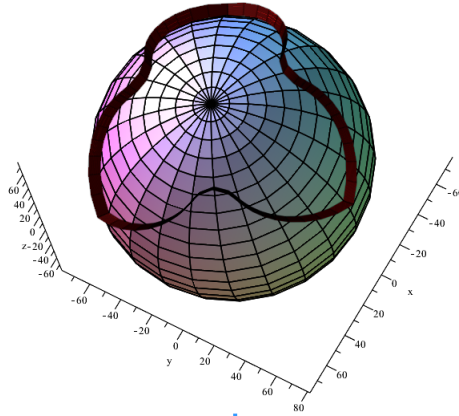


Fig. 4. Conic surface defining the spherical cam-profile intersecting the sphere on which the spherical mechanism is based

value needs to be calculated for the *radius of curvature*, denoted by  $\rho$ . As explained by McCarthy et al. [2], the *radius of curvature* is related to the position vector  $\mathbf{s}_p$  of the pitch curve is given by

$$\tan \rho = \frac{\|\mathbf{s}'_p\|^3}{\mathbf{s}_p \times \mathbf{s}'_p \cdot \mathbf{s}''_p} \quad (6)$$

In Eq.(6), the prime denotes the first derivative with respect to the input angle  $\psi$ , the double prime the second derivative. *Undercutting* takes place when the radius of curvature of the cam-profile projection on the sphere vanishes, which can be obtained from the relation given in Eq.(6), if the numerator is equated to zero, i.e., when

$$\frac{\partial \mathbf{s}_p}{\partial \psi} = \mathbf{0} \quad (7)$$

The minimum radius of curvature occurs at a value of  $\psi$  where the roller axis lies closest to the cam axis. This value is  $\psi = \pi/M$ . Thus, Eq.(7) leads to

$$\tan \bar{\alpha}_3 = \frac{N}{M} \quad (8)$$

Here  $\bar{\alpha}_3$  denotes the critical value of  $\alpha_3$ , the angle subtended by the arc representing the roller carrier. This value just gives an upper bound for  $\alpha_3$  to avoid undercutting. The plots of the cam profile are obtained for various values of  $\alpha_3$  ( $< \bar{\alpha}_3$ ); the one with a smooth profile that ensures undercutting-avoidance, is chosen.

#### 4. PRESSURE ANGLE

The pressure angle of spherical cam mechanisms is the angle between the line of action of the force applied by the driver element and the direction of the velocity of the contact point of the driven element. The positive and the negative actions of the cam mechanism are first described, then expressions for the pressure angle in both cases are obtained.

##### 4.1. Reversible Action

The spherical cam mechanism considered in this report is reversible, which means that both cam and roller-carrier can play the role of the driver, the other of the driven element. Two types of action and the

corresponding expressions of the pressure angle are explained below.

#### 4.1.1. Positive Action

In this case the cam drives the roller-carrier. The driving force being applied by the cam, the pressure angle is defined as that between the line-of-action of this force and the direction of the velocity vector of the contact point on the driven roller-carrier, as shown in Fig. 5.

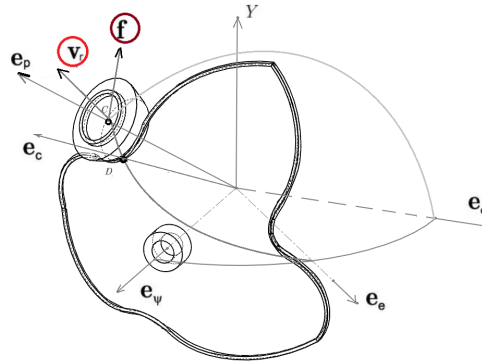


Fig. 5. Pressure Angle for positive action

We thus can obtain the relation for the pressure angle under positive action, denoted by  $\mu_p$ , as

$$\tan \mu_p = \frac{\| \mathbf{f} \times \mathbf{v}_r \|}{\mathbf{f} \cdot \mathbf{v}_r}$$

Here  $\mathbf{f}$  is the unit vector along the force applied by the cam, while  $\mathbf{v}_r$  is the velocity vector of the roller-carrier at the intersection of roller axis and unit sphere.

These vectors are given by  $\mathbf{f} = \mathbf{e}_p \times (\mathbf{e}_p \times \mathbf{e}_c)$  and  $\mathbf{v}_r = \mathbf{e}_p \times \mathbf{e}_\phi$ .

#### 4.1.2. Negative Action

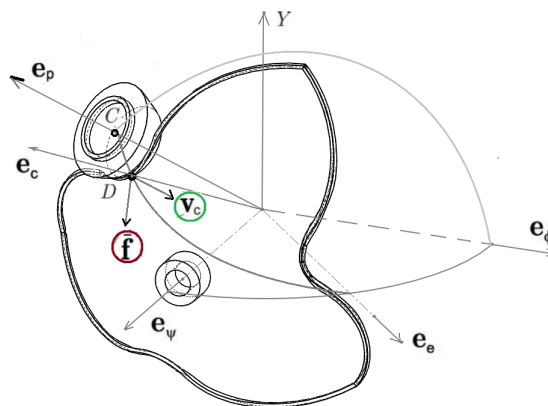


Fig. 6. Pressure angle for negative action

In this case the roller-carrier drives the cam. The direction of the force vector and that of the velocity vector for the cam is shown in the Fig. 6.

Now we have the expression below for the pressure angle, denoted by  $\mu_n$ .

$$\tan \mu_n = \frac{\|\bar{\mathbf{f}} \times \mathbf{v}_c\|}{\bar{\mathbf{f}} \cdot \mathbf{v}_c}$$

Here  $\bar{\mathbf{f}}$  is the unit vector parallel to the force applied by the roller-carrier and  $\mathbf{v}_c$  is the velocity vector of the cam at the intersection of the generatrix of the cam conical surface with the unit sphere. Expressions for these vectors are given as  $\bar{\mathbf{f}} = \mathbf{e}_c \times (\mathbf{e}_c \times \mathbf{e}_c)$  and  $\mathbf{v}_c = \mathbf{e}_\phi \times \mathbf{e}_c$ .

#### 4.2. Pressure Angle Plots

The distribution of the pressure angle depends on three parameters,  $M$ ,  $N$  and angle of the roller-carrier,  $\alpha_3$ . From the singularity-analysis, the profile is found to have a smoother shape with an increase in the number of rollers. Negative action is implemented to drive the spherical cam mechanism. Pressure angle plots are obtained for negative action; it is found that the pressure angle grows with the number of rollers. Thus, the optimum number of rollers is chosen to be four. Typical plots for pressure-angle distribution are shown in Fig 7.

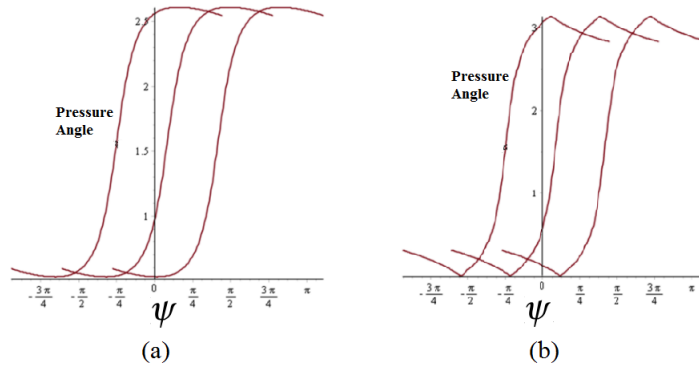


Fig. 7. Pressure-angle distribution for negative action with: (a)  $M = 3$ ;  $N = 4$ ;  $\alpha_3 = \tan^{-1}(M/N) - 0.0174$ ; (b)  $M = 3$ ;  $N = 4$ ;  $\alpha_3 = \tan^{-1}(M/N) - 0.0348$ ;

### 5. CONTACT RATIO

The contact ratio for cam mechanisms  $m_p$  is defined similar to gears, as the ratio of the action angle  $\psi_a$  to the pitch angle  $\psi_p$  as explained by Bai and Angeles [1]. If  $\psi_a$  is defined as the angle of rotation of the cam for which it is in contact with a single roller, and for the pitch angle we have  $\psi_p = 2\pi/M$ , then the following relations are obtained

$$m_p = \frac{\psi_a}{\psi_p} = \frac{2\pi/M + 2\sigma}{2\pi/M} = 1 + \frac{M\sigma}{\pi} \quad (9)$$

A contact ratio greater than 1 ensures continuous roller-cam contact and a pure rolling motion between roller and cam upon driving the cam mechanism.

### 6. A PITCH-ROLL JOYSTICK

#### 6.1. Design of Joystick

The design of the pitch-roll joystick described here utilizes a spherical cam mechanism with the layout of a differential mechanism, there by offering two degrees-of-freedom (*dof*). One *dof*, the rolling, is about the axis of the roller-carrier, the second, or pitching, about the cam axis.

The plots for various cam-profiles of a cam with three lobes are obtained for various values of number of rollers  $N$  and angle  $\alpha_3$ . With an increase in the number of rollers the profile is found to be smoother. Negative action is implemented to drive the spherical cam mechanism. Pressure angle plots are obtained for negative action; it is found that the pressure angle grows with the number of rollers, which is chosen as four.

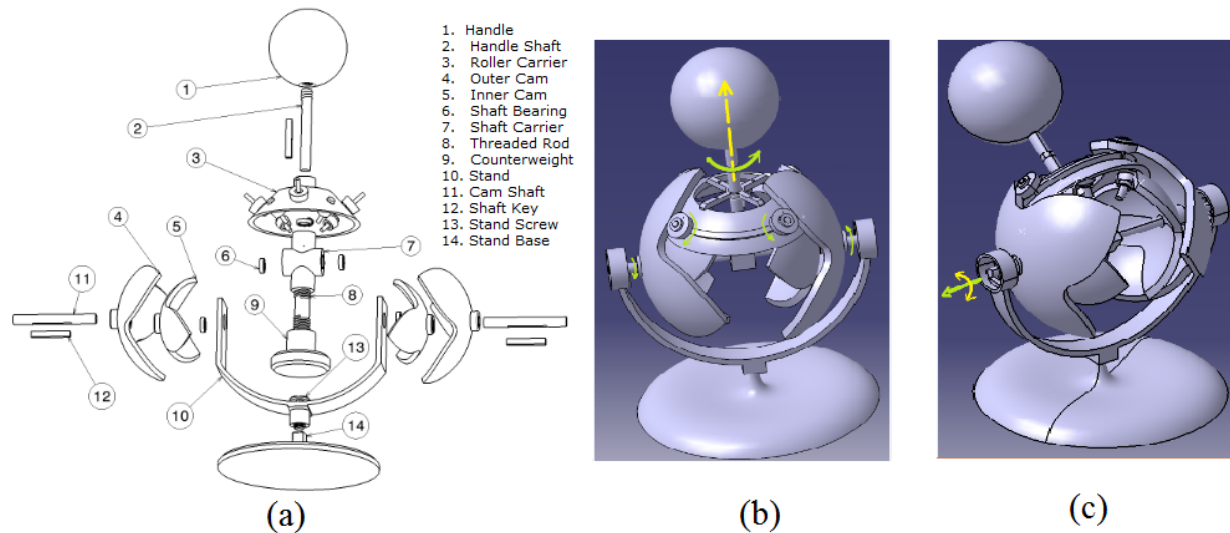


Fig. 8. (a) Exploded view of the joystick assembly; (b) Illustration of rolling; (c) Illustration of pitching

The joystick comprises two pairs of spherical cams placed in a diametrically opposed layout. Each pair has an inner, smaller cam and an outer, larger cam. These two cams form a set of coaxial conjugate cams that are keyed rigidly into a single cam shaft and positioned at a  $60^\circ$  phase angle. This means that the crest of a lobe of one of the cams lies at the trough of the lobe of the corresponding conjugate cam. The roller-carrier rigidly attached to the handle to which it is keyed provides two *dof*. The carrier holds two sets of four rollers; one outer set and one inner set. The outer rollers engage with the outer cams, the inner rollers with the smaller, inner cams. The roller-stands that carry the rollers are press-fitted on holes on the conical surface of the roller-carrier plate. Each roller is composed of a roller cup in the shape of a frustum with a cylindrical hole that carries a suitable bearing.

The size of the bearings used for the rollers (especially the inner rollers) are the bearings with smallest outside diameter. The radii of the conjugate cams and, consequently, the size of the other components of the joystick and, thus, the size of the entire assembly are decided based on the size of easily available standard bearings of the smallest outside diameter without going into the precision bearing category. The corresponding smaller cam diameter is calculated and specified as 100 mm, the bigger cam diameter as 136 mm. The roller-carrier is designed as a frustum shell open at the circle with bigger diameter. The surface of the roller-carrier is designed in such a way that once the roller-stands are press-fitted in the holes on this surface, the stands are at an angle equal to  $\alpha_3$ . The value of  $\alpha_3$  is set at  $48.13^\circ$  which is obtained using Eq.(8).

The spherical nature of the driving cams make a gimbal frame suitable for mounting the cams in a coaxial manner as widely used in joystick design, and one such example is the two *dof* joystick developed by Li et al. [11]. The diametrically opposed two cam pairs are keyed to separate shafts; these cam-shaft are coaxially mounted on a shaft-carrier, the central element of the joystick, which carries all the shafts and ensures their proper orientation w.r.t. each other and thus the proper engagement of the rollers on roller-carrier with the cam lobes. The cam-shafts are mounted on one side on the gimbal frame with the help of ball bearings; on

the other end they are keyed to the shaft-carrier. The roller-carrier is mounted on a shaft that is keyed to the shaft-carrier so that its axis is orthogonal to that of the cam-shafts. The shaft-carrier has a counter-weight attached to it with the help of a threaded shaft in a diametrically opposite position w.r.t. the roller-carrier.

The shaft to which the roller-carrier is keyed carries a spherical handle of a size suitable for a proper grip by an adult human hand. The gimbal frame carrying the shaft-carrier with the mounted cams and roller-carrier is bolted to a disk-shaped stand for stable operation of the joystick. The exploded view of the joystick assembly is displayed in Fig. 8(a), the various parts comprising the mechanism being enumerated in the same figure.

## **6.2. Kinematics of the Pitch-Roll Joystick**

The spherical cam mechanism implemented in the pitch-roll joystick functions under negative action. The handle is attached to the roller-carrier. When torque is applied on the handle, the roller-carrier drives the two sets of conjugate cams.

### **6.2.1. Rolling**

For the rolling of the joystick the torque is applied about the roller-carrier axis, which rotates about the handle axis while the rollers roll w.r.t. the cams, on the conical surfaces of their corresponding cam from the set of conjugate cams (the bigger, outer cam and the smaller, inner cam). The two sets of cams rotate in opposite directions. One of the configurations of the joystick while performing pitching motion is depicted in Fig. 7(b)

At one time, there are three contact points between one set of coaxial conjugate cams and their corresponding rollers. For the whole mechanism, there are a total of six contact points. In one half of the rotation cycle of the roller-carrier, the outer cams have two contact points, each with their neighboring outer rollers; for the inner cams, each has one contact point with the inner rollers. In the other half, the inner cams have two contact points each, whereas the outer cams have just one contact point each. The reason why there is a different number of contact points is that the inner and outer cams lie at a  $60^\circ$  phase angle.

### **6.2.2. Pitching**

The pitching of the joystick takes place when the torque is applied about the cam axis. In this case, the motion between the rollers of the roller-carrier and the corresponding cams becomes locked. The two pairs of conjugate cams then move in the same direction. The contact points do not change during this motion; they thus remain the same as if they were in the initial configuration at the point of initiation of pitching. One of the configurations of the joystick while performing pitching motion is depicted in Fig. 7(c).

## **7. CONCLUSIONS**

The spherical cam mechanism provides a sound alternative to bevel gears for developing a pitch-roll joystick that targets haptics applications. The advantages of lower backlash and higher stiffness can compensate for the higher cost of manufacturing incurred in the case of cam mechanisms. These advantages are guaranteed by a continuous roller-cam contact and a pure rolling motion between roller and cam when driving the joystick handle. The size of the joystick based on a spherical cam mechanism is in agreement with that proposed by ergonomic studies on hand-driven joystick devices. For a joystick of this size, the feasibility of machining the small components of the joystick assembly becomes an issue. Such a joystick is envisioned to be implemented as a haptic device. Future work should include augmenting the joystick with a force feedback system. Encoder motors capable of producing force feedback can be coupled with the cams. The torque sensors can be placed along the axis of the roller-carrier handle. Another task is developing haptics algorithms for such a joystick. Apart from employing the joystick as a haptic device, it can also be used

as a control device for manipulators, for example, for pick-and-place robots used in the packaging industry. The independent pitch and roll motions of the joystick can lead to applications where manipulators need to perform distinct rotations about two perpendicular axes.

## REFERENCES

1. Bai, S. and Angeles, J., The design of spherical multilobe-cam mechanisms, *Journal of Mechanical Engineering Science*, Vol.223, No. 3, pp. 473–482, 2009.
2. McCarthy J. M. and Roth B., Instantaneous properties of trajectories generated by planar, spherical, and spatial rigid body motions, *ASME Journal of Mechanical Design*, Vol. 104, No. 1, pp. 39–51, 1982.
3. Gonzalez-Palacios M. A. and Angeles J., *Cam Synthesis*, Kluwer Academic Publishers, 1993.
4. Nutbourne A. W. and Martin R. R., *Differential Geometry Applied to Curve and Surface Design, Vol.1: Foundations*, 1988 (Ellis Horwood Ltd., West Sussex).
5. Rutter J. W., *Geometry of Curves*, CRC Press LLC, Florida, 2000.
6. Wei E. J., Lai H. Y., Chen C. K., Machine tool setting for the manufacturing of spherical cams, *Journal of Material Processing Technology*, Vol. 100, pp. 147–155, 2000.
7. Karwowski W., *International Encyclopedia of Ergonomics and Human Factors*, Taylor & Francis, 2001.
8. Agronin, M. L., The design of a nine-string six-degree-of-freedom force-feedback joystick for telemanipulation, *Proceedings of the Workshop on Space Telemetry and Robotics*, Vol. 2, pp. 341–348.
9. Hayusmans, M. A., de Looze M. P., Hoozemans M. J. M., van der Beek A. J., van Dieën J. H., The effect of joystick handle size and gain at two levels of required precision on performance and physical load on crane operators, *Ergonomics*, 49:11, pp. 1021-1035, Taylor & Francis, 2007
10. Takemoto A., Yano K., Miyoshi T., Terashima K., Operation assist control system of rotary crane using proposed haptic joystick as man-machine interface, *Proceedings of the 20004 International Workshop on Robot and Human Interactive Communication*, pp. 533–538, 2004.
11. Li W. H., Liu B., Kosasih P. B., Zhang X. Z., A 2-DOF MR actuator joystick for virtual reality applications, *Sensors and Actuators A: Physical*, Vol. 137, No. 2, pp. 308-320, 2004.